ADVANCED ELECTRONIC MATERIALS
www.advelectronicmat.de

Band Bending Engineering at Organic/Inorganic Interfaces Using Organic Self-Assembled Monolayers

Oliver T. Hofmann and Patrick Rinke*

Adsorbing strong electron donors or acceptors on semiconducting surfaces induces band bending, whose extent and magnitude are strongly dependent on the doping concentration of the semiconductor. This study applies hybrid density-functional theory calculations together with the recently developed charge reservoir electrostatic sheet technique to account for charge transfer from the bulk of the semiconductor to the interface. This study further investigates the impact of surface-functionalization with specifically tailored self-assembled monolayers (SAMs). For the example of three chemically-similar SAMs, that all bond to the ZnO surface via pyridine docking groups, it is shown that the SAMs introduce shallow or deep donor levels that pin the band bending at the position of the SAM's highest occupied molecular orbital. In this way, the magnitude of the induced band bending can be controlled by the type of SAM, to a point where the doping-concentration dependence is completely eliminated.

1. Introduction

Organic photovoltaic cells and light-emitting devices require at least one transparent electrode such that light can reach or leave the organic material in which it is produced from or converted to electricity. Although in principle such electrodes can be realized using nanoscale metals, it is more convenient to use doped, large band-gap transparent conductive oxides, such as ZnO. Often, these optically active organic materials are not in direct contact with ZnO. Instead, molecular electron acceptors are sandwiched between the optical organic material and ZnO, either because the electron acceptors are part of the active organic materials (e.g., fullerenes in photovoltaic cells[1–4]) or to modify the work function of ZnO, and therefore the charge injection and extraction barriers (as in the case of, e.g., CuPc,[5] perylene-2,3,9,10-tetracarboxylic dianhydride (PTCDA),[5,6] or F4TCNQ[7]).

Dr. O. T. Hofmann
Graz University of Technology
Institute of Solid State Physics
NAWI Graz, Petersgasse 16/II, 8010 Graz, Austria
E-mail: o.hofmann@tugraz.at
Dr. O. T. Hofmann, Prof. P. Rinke
Fritz Haber Institute of the Max Planck Society
Faradayweg 4-6, 14195 Berlin, Germany
Prof. P. Rinke
COMP/Department of Applied Physics
Aalto University
P.O. Box 11100, Aalto FI-00076, Finland

DOI: 10.1002/aelm.201600373

The electron acceptors receive charge from the semiconductor until their acceptor levels are energetically in resonance with the Fermi energy. The resulting ground-state charge transfer across the interface gives rise to the formation of a space-charge region and associated band bending. This space-charge region can affect the charge-transport properties across the interface and significantly weakens the binding between substrate and adsorbate.[8] The spatial extent and the magnitude of the band bending depend on the amount of charge-transfer from the bulk to the adsorbate as well as on the bulk doping concentration and profile. Experimentally, those parameters are often challenging to control and not always well known. Moreover, they are subject to change during device operation, e.g., due to migration of charged defects, impeding the long-term stability of (opto)electronic devices.

When the electron affinity of the adsorbate is larger than the substrate's work function, i.e., when the lowest unoccupied molecular orbital (LUMO) is below the Fermi-energy (E_F) as schematically shown in **Figure 1**a, the bulk crystal donates electrons to the adsorbate. The ensuing dipole moment ($\Delta\Phi$) shifts the now partially occupied LUMO upward in energy until it is in resonance with the Fermi-energy.[9,10]

The overall interface dipole, $\Delta\Phi$, is often divided into a band bending contribution $\Delta\Phi_{BB}$ (i.e., the long-range, quasi-parabolic potential within the substrate), and a surface-dipole contribution $\Delta\Phi_{SD}$ (the approximately linear potential change in the "empty" space between substrate and adsorbate), as indicated in Figure 1b. The relative contribution of $\Delta\Phi_{BB}$ and $\Delta\Phi_{SD}$ depends strongly on the doping concentration of the substrate.[8] In principle, for low doping concentrations and strong electron acceptors, band bending could be as large as the total band gap of the substrate (≈3.5 eV in ZnO). In practice, however, $\Delta\Phi_{BB}$ is almost always limited by the presence of defect states at or near the surface, such as oxygen vacancies,[11–13] provided they are present in sufficient concentrations.

Since the type and concentration of these defects is difficult to control, band bending is typically hard to engineer. In this article, we use these defect states as an analogy to demonstrate a new concept that uses properly designed, covalently attached self-assembled monolayers (SAMs) to act like surface defects that limit band bending at desired values. In order to do so, the highest occupied molecular orbitals (HOMOs) of these SAMs need to lie within the band gap of the inorganic substrate. This

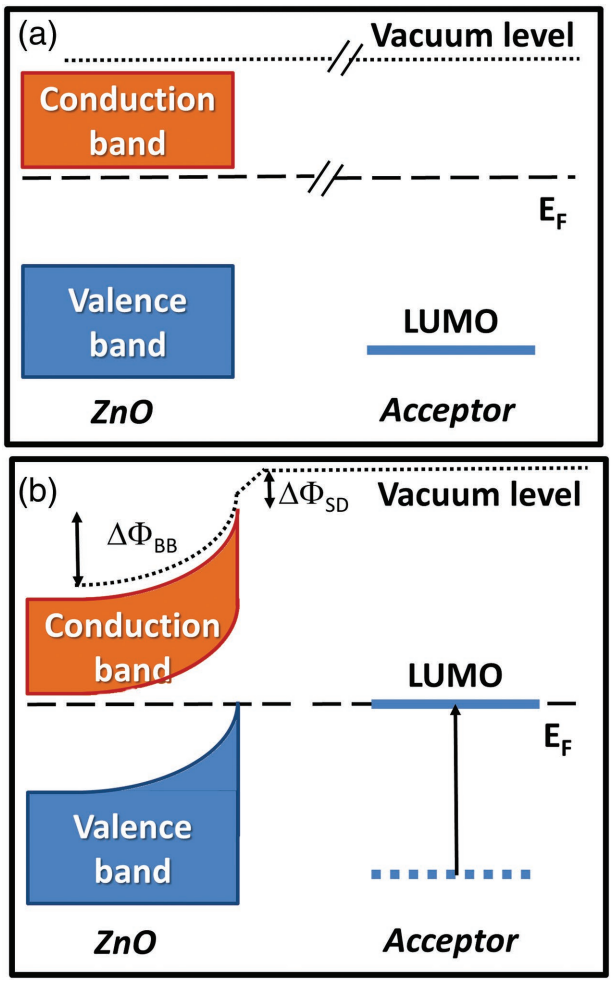

Figure 1. Schematic level alignment at a semiconductor/organic interface a) prior and b) upon interaction of an acceptor with an n-type semiconductor (here ZnO). $\Delta\Phi_{BB}$ denotes the change in the electrostatic potential due to band bending, $\Delta\Phi_{SD}$ is the surface dipole.

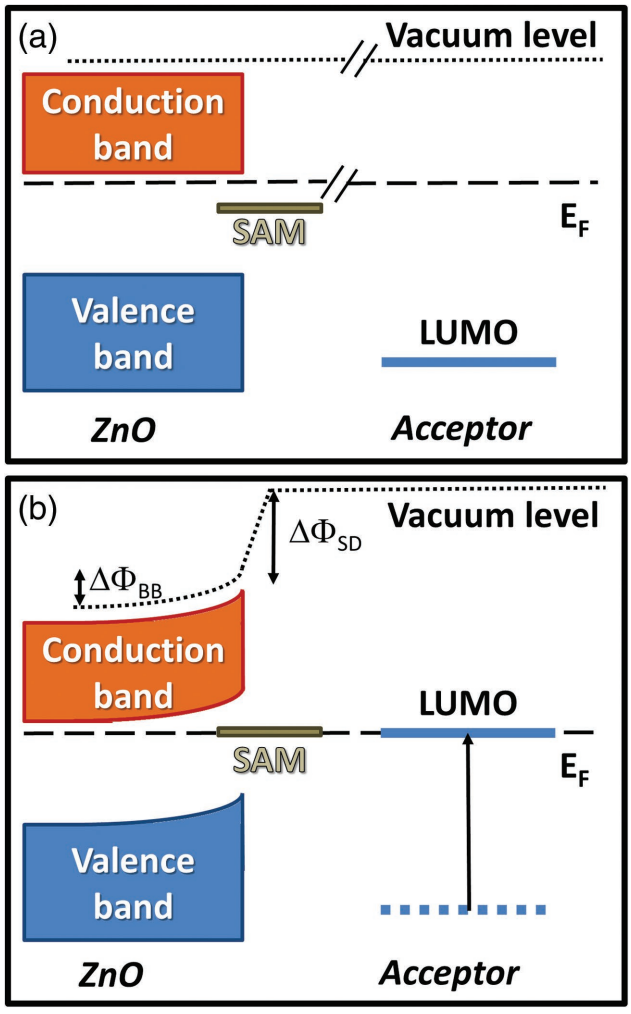

Figure 2. Schematic level alignment at a semiconductor/SAM/organic interface a) prior and b) upon interaction. $\Delta\Phi_{BB}$ denotes the change in the electrostatic potential due to band bending, $\Delta\Phi_{SD}$ is the surface dipole.

situation is schematically shown in **Figure 2**. Upon contact with the organic adsorbate, band bending will emerge until it shifts the SAM-HOMO up to the Fermi-energy. As soon as the SAM-HOMO becomes resonant with the Fermi energy, charge transfer from the SAM toward the adsorbate opens up as an additional electron-transfer channel, thereby inhibiting any further band bending. The SAM thus acts akin to deep donor states. While conventional deep donor states are usually intrinsic to a material and thus found at fixed energies, organic SAMs put the vast toolbox of organic chemistry at our disposal to tune the pinning energy of the SAM. It is possible to design SAMs with states at desired energies and thereby control the energy landscape and the exact amount of band bending at the interface. With this design principle it would be possible to create organic electronic devices that are less dependent on the growth conditions of the semiconductor substrate (and, hence, its doping concentration) and that exhibit better long-term stability.

To demonstrate this concept, we study the interface between a ZnO($10\bar{1}0$) surface functionalized with a SAM and a tetracyano-quinodimethane (TCNQ) layer. TCNQ is a typical, strong electron acceptor that is frequently used for level-alignment studies, in particular in conjunction with other organic materials.[14–22] To functionalize the interface between ZnO and TCNQ, we consider three organic SAMs: doubly reduced viologen (Vio), diamino-4-phenyl-pyridine (DAPP), and 2,5-*para*-phenylpyridine (PPP). These three molecules, whose chemical structures are shown in **Figure 3**, are listed here in order of their increasing ionization potential (decreasing HOMO, vide infra). In all molecules we used pyridine as docking group, which has been shown to form stable (2 × 2) patterns on ZnO($10\bar{1}0$) without inducing appreciable etching.[23–25] Moreover, a full monolayer of pyridine reduces the work function of ZnO($10\bar{1}0$) by almost 3.0 eV[25] and therefore increases the charge-transfer across the interface, amplifying the effect that we intend to demonstrate here. It is worthwhile mentioning that the introduction of these polar SAM layers does not affect the final work function that results from TCNQ deposition,[26] changes in the geometric structure notwithstanding. For the sake of demonstrating the concept, we consider atomistically clean, defect-free ZnO. Accounting for additional deep donor states, as done e.g.,

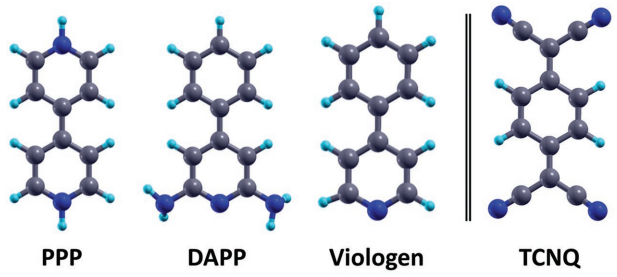

Figure 3. Chemical structure of the molecules used in this work. Para-phenylenepyridine (PPP), 2,5-diamino para-phenylenepyridine (DAPP), and Viologen (Vio), serve as surface functionalization. Tetracyanoquinodimethane (TCNQ) is the electron acceptor. Grey spheres denote carbon, blue spheres nitrogen atoms, and cyan spheres hydrogen atoms.

in ref. [6], is straightforward but would unduly complicate the calculations and the interpretation of the results.

All studies were performed using density functional theory (DFT) in the repeated-slab approach, employing the Heyd–Scuseria–Ernzerhof (HSE) hybrid functional family.[27,28] We increase the fraction of exact exchange to 40% to improve the description of the band gap as well as the valence band width of ZnO (as demonstrated in refs. [25,29,30]). We have previously reported that the choice of the functional does not affect the interface dipole generated by the adsorption of pyridine-SAMs.[25] To account for long range van der Waals interactions, we used the vdW-TS[31] scheme with an appropriate parameterization for metal oxides.[32] Band bending and doping are treated using a simplified version of the charge reservoir electrostatic sheet technique (CREST).[33,34] In short, CREST simulates the space-charge region by a negatively charged sheet placed on the backside of the slab. The charge and position of the sheet is determined self-consistently, using only the substrates doping concentration N_D and its dielectric constant as parameters. Within the quantum-mechanically treated ZnO slab, we accounted for the variable n-type doping by means of the virtual crystal approximation.[35] More details are given in the Experimental Section at the end of this paper.

2. Results and Discussion

2.1. TCNQ on Nonfunctionalized ZnO

To establish a reference, a useful first step is to examine the adsorption of TCNQ on the pristine, unaltered ZnO surface. We consider two morphologies: (1) a low-density structure in which TCNQ molecules are adsorbed face-on (i.e., flat lying), and (2) a high-density structure in which TCNQ molecules adsorb edge on (i.e., upright standing). Our calculations show that TCNQ can assume several adsorption geometries on ZnO(10-10) that are energetically very close to each other. Hence, we would expect that in experiments, TCNQ would probably form disordered films. Since a full structure search or an investigation of disordered films is beyond the scope of the present paper, the two ordered morphologies can be regarded as "extreme cases" of different adsorption structures. Hereafter, we will focus on the upright standing TCNQ film, shown as inset in **Figure 4**,

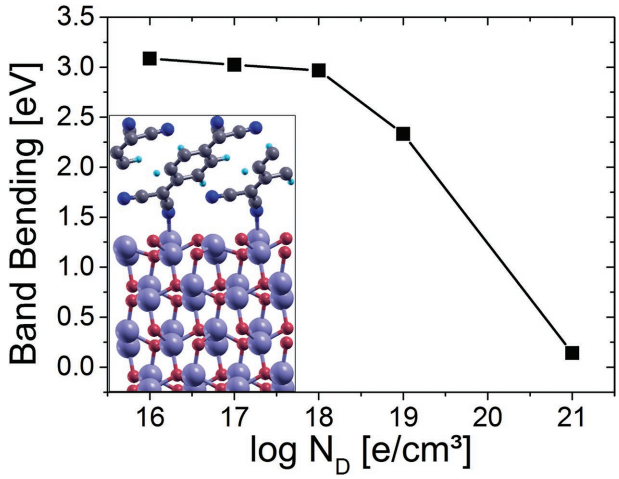

Figure 4. Adsorption-induced band bending as a function of the substrate doping concentration for an upright-standing TCNQ film on the ZnO(10-10) surface.

since TCNQ also assumes a similar adsorption geometry upon adsorption on the self-assembled monolayers (see below). It should be emphasized, however, that the doping dependence of the adsorption-induced band bending agrees qualitatively for the flat-lying and the upright-standing geometry.

The band-banding contribution to the adsorption-induced work-function change is shown as a function of the ZnO doping concentration in Figure 4. We chose to define band bending by the change of the onset of the ZnO valence band (with respect to the Fermi-energy) of the ZnO/SAM/TCNQ system relative to the pristine ZnO surface. We find that the work function after adsorption (≈6 eV) is essentially independent of the bulk doping concentration, as previously observed for F4TCNQ on the polar ZnO surfaces.[7,8] At the lowest considered doping concentration ($N_D = 10^{16}$ e cm^{-3}), the band bending is $\Delta\Phi_{BB} = 3.1$ eV and thus of the same order of magnitude as the band gap. For larger doping concentrations, $\Delta\Phi_{BB}$ becomes smaller. The change of $\Delta\Phi_{BB}$ with N_D is relatively small between 10^{16} and 10^{18} e cm^{-3}. For larger N_D, however, $\Delta\Phi_{BB}$ decreases exponentially, until it vanishes for degenerately doped ZnO ($N_D = 10^{21}$ e cm^{-3}). The doping concentration of natively doped ZnO is ≈10^{17} e cm^{-3}.[36] The large sensitivity of $\Delta\Phi_{BB}$ to N_D at this value further illustrates the importance of controlling the band bending by surface functionalization.

2.2. Surface Functionalization of ZnO

To demonstrate the impact of specifically customized self-assembled monolayers on the level alignment between TCNQ and ZnO, we consider three different archetypes, which are characterized by the position of the molecular HOMO with respect to the ZnO band gap.

PPP serves as our "blind-test." Its ionization energy is sufficiently large that its DFT HOMO lies below the valence band maximum (VBM) of ZnO, and its gap is large enough such that its LUMO is located above the conduction band minimum of ZnO. In other words, PPP does not induce states in the ZnO

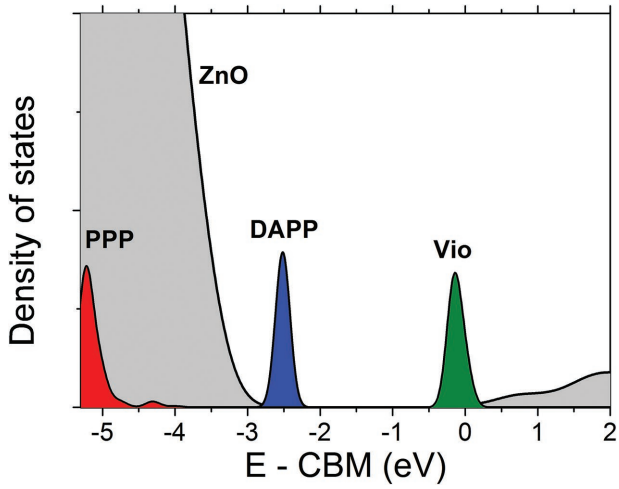

Figure 5. Level alignment between ZnO(10-10) and the three SAMs PPP (red), DAPP (blue), and Vio (green). For clarity, only the HOMO of the SAMs is shown. A density of states with all molecular contributions can be found in the Supporting Information.

band gap, as shown in **Figure 5**. The second molecule in our study is DAPP. Although this molecule is chemically very similar to PPP, the two amine groups and their corresponding dipole moments decrease the ionization potential of DAPP significantly. On the surface, the HOMO of DAPP is found in the ZnO gap, ≈2.3 eV below the Fermi energy (E_F). Finally, Vio is a particular strong electron donor[37–40] due to its quinoid structure. It exhibits a HOMO 0.1 eV below the conduction band edge and thus directly at the Fermi energy.

Our calculations indicate that all three SAMs adopt a similar morphology on the surface, as shown in the Supporting Information. In analogy to the interaction of unsubstituted pyridine with ZnO(10-10),[23–25] all molecules adsorb with the nitrogen lone pair situated above a surface Zn atom. The energetically most stable packing density (at 0 K and omitting the zero-point energy) is found at 5.8 molecules per nm^2, which amounts to one molecule bonded to every second surface Zn atom. Tighter molecular packing is less stable due to steric repulsion between the molecules in the layer.

In experiments, ZnO is typically n-type doped,[41] with its Fermi level ≈200 meV below the conduction band onset. Since all SAMs considered here are electron donors, they potentially introduce downward band bending, which is limited by the difference between the conduction band and E_F. We have recently verified for pyridine that our surface slab models contain enough ZnO layers to capture this downward band bending.[25] The interface dipole induced by the adsorption of the SAMs causes a strong reduction of the work function of the substrate from 4.6 eV (pristine) to 1.2 eV (Vio), 2.9 eV (DAPP), and 1.7 eV (PPP). (Note that the work-function modification induced by the SAMs does not correlate with the ionization potential because of the molecules' inherent dipole moment.) Intuitively, one might assume that the different work function of the ZnO/SAM system will impact the level alignment of subsequently deposited TCNQ. However, for molecules which are in the so-called Fermi-level pinning region (i.e., where a molecular state is in resonance with the Fermi-energy after adsorption), we have previously shown that any dipole that is spatially located between the charge reservoir (here: ZnO) and the adsorbate (TCNQ) has no net effect on the final work function;[26] a claim that, as will be shown in the following, is corroborated by the observation that the work-function after TCNQ deposition is essentially independent of the underlying SAM.

2.3. Adsorption of TCNQ on Functionalized ZnO

On all three SAMs, we find that TCNQ adopts a roughly upright-standing geometry, shown in the Supporting Information. If there would be no interaction between the TCNQ film and the ZnO/SAM system, the TCNQ LUMO would be located 6.2–6.5 eV below the vacuum level in our calculations. The difference occurs due to the slightly different inclination of the TCNQ molecules with respect to the surface normal.[42] The LUMO of TCNQ is thus low enough that even if we assume vacuum level alignment (i.e., the noninteracting limit) it would be located below the HOMO of Vio and DAPP, but not of PPP. Furthermore, it is always below the conduction band onset of ZnO. Therefore, electron transfer from the inorganic substrate to TCNQ should be expected in all three cases.

To understand the processes occurring upon adsorption of TCNQ on the SAM/ZnO surfaces, it is instructive to first consider the "metallic limit." "Metallic limit" here refers to a situation in which the substrate is so strongly doped such that the bands are practically flat and the little bit of (upward) band bending induced by electron transfer from "bulk" ZnO to its surface is confined to a few Å. In other words, all band bending is completely captured in a slab calculation with only eight ZnO layers. Here we used a doping concentration of 10^{21} e cm^{-3} to achieve this metallic limit. The resulting level alignment, shown in **Figure 6**a–c, shows (i) that there is no appreciable band bending, illustrated by the observation that the conduction band edge of the topmost layers is still below the Fermi energy, and (ii) that the TCNQ LUMO shifts into resonance with the Fermi-energy in all three cases. Consequently, we observe a fractional filling of the (former) TCNQ LUMO upon adsorption. (We note that no hybrid states form since there is no wave-function overlap between ZnO and the TCNQ molecules. In previous work, we showed that in such cases integer charge transfer would be expected.[43] The fact that we observe partial and not integer charge transfer in our calculations in this work is partly a result of the self-interaction error still present in the hybrid functional we use[43–45] and partly due to the small lateral size of the unit cell that does not permit charge localization on individual molecules. The distinction between integer and fractional charge transfer does not affect our results here. Nonetheless, the partial filling in our calculations should be interpreted as an ensemble-average of charged and neutral TCNQ molecules, in the same sense as the virtual crystal approximation represents an ensemble average of substrate and dopant atoms.) A Mulliken charge analysis shows that each TCNQ molecule accepts ≈0.60 e on Vio, 0.13 e on DAPP, and 0.15 e on PPP.

The combined systems exhibit total work functions of 6.3–6.8 eV, agreeing well with the LUMO-energy of the noninteracting monolayer. We emphasize again that because the

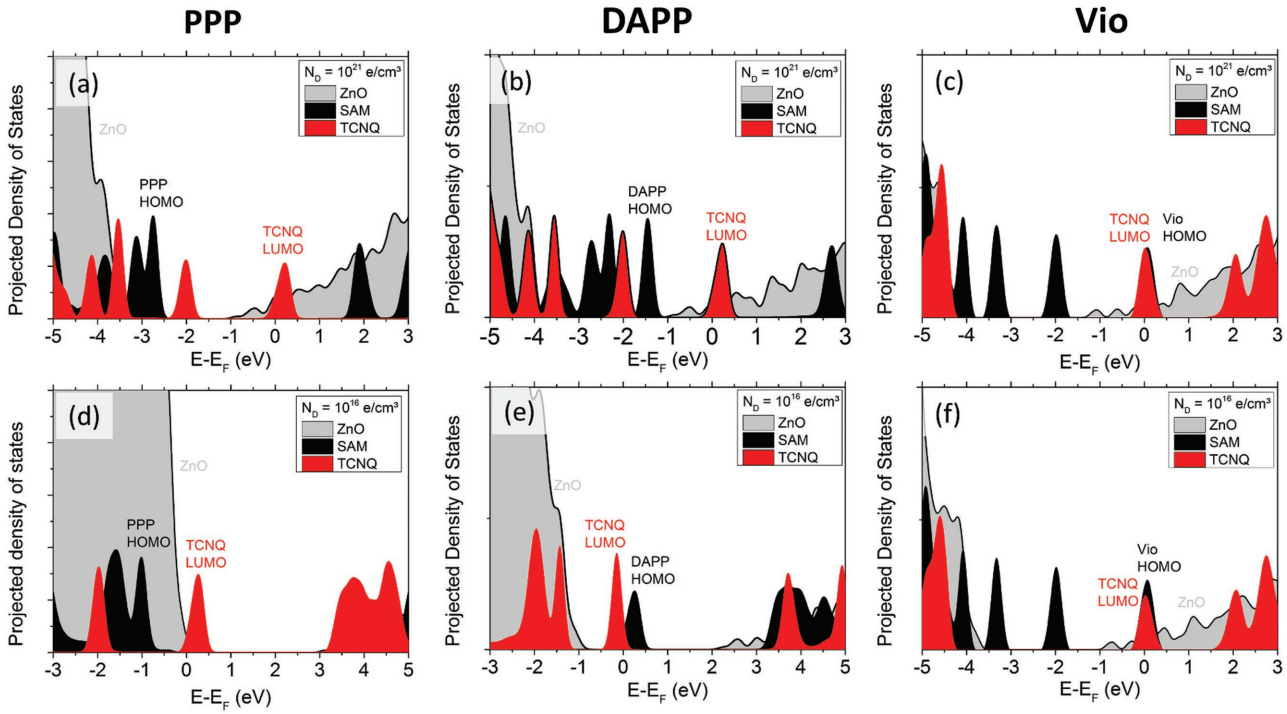

Figure 6. Level alignment for TCNQ on modified ZnO. a–c) The level alignment upon contact with the TCNQ crystal for metallic doping. d–f) The level alignment upon contact for a doping concentration of 10^{16} e cm^{-3}. For ZnO only the projection onto the four topmost double layers is shown.

SAM is located between the charge reservoir (ZnO) and the pinned system (TCNQ), its dipole moment has essentially no impact on the final work function of the pinned system.[26] The interface dipole also shifts the states of the SAM significantly upward in energy. For Vio, the HOMO is now in resonance with the TCNQ LUMO. This shows that Vio directly donates charge to TCNQ and explains why the LUMO occupation is so much higher than for the other two SAMs. DAPP shows an increase of the HOMO energy from 2.3 to 1.3 eV below E_F, with the HOMO still being significantly below the TCNQ LUMO. Also PPP shows a significant increase of its HOMO energy, which is now found in the ZnO gap, but still far below the TCNQ LUMO (see Figure 6).

As a next step, we consider more realistic doping concentrations. In particular for low doping concentrations, the spatial extent of the depletion region can reach macroscopic dimensions. In general, it is not possible to model slabs which are sufficiently large to capture the whole region. We therefore employ the CREST method.[33]

In Figure 6d–f, the level alignment for all three systems is shown exemplarily for a doping concentration of 10^{16} e cm^{-3}. The ZnO/Vio/TCNQ system does not exhibit any band bending, since the HOMO of Vio lies directly at the Fermi-energy already prior to adsorption, and hence, does not require any band bending to induce charge-transfer from the SAM to the adsorbate. For ZnO/DAPP, the HOMO was initially 2.4 eV below the Fermi-energy. DAPP is thus only able to contribute to charge transfer to TCNQ once its HOMO has been shifted to the Fermi-energy by virtue of band bending, i.e., at a band bending value that corresponds to the difference of the HOMO to the Fermi energy prior to interaction. Upon TCNQ adsorption, we observe band bending of ≈2.4 eV, which indeed moves the DAPP-HOMO into resonance with the Fermi energy, where band bending subsequently pins. We emphasize here once again that our model for the ZnO slab does not include other deep donor states except for those induced by the SAM. In reality, it is likely that such states would be present and pin the band bending already at a smaller value. Nonetheless, the results nicely corroborate the fundamental mechanism proposed in Figure 2. Conversely, for the ZnO/PPP system the SAM-HOMO is below the VBM of ZnO. Once band bending is developed, the valence band reaches the Fermi-energy before the PPP-HOMO does, and the band bending is only limited by the magnitude of the ZnO band gap.

To ascertain the stability of the result, we have calculated the level alignment for doping concentrations between 10^{16} and 10^{19} e cm^{-3}. The resulting band bending is depicted in **Figure 7**. Within the calculated doping range, there is no band bending for ZnO/Vio. For ZnO/DAPP, band bending is mostly constant between 10^{16}–10^{18} e cm^{-3}, and slightly decreases at higher doping concentrations. For PPP, band bending always amounts to the maximally achievable value, i.e., the ZnO band gap value of 3.5 eV in our calculations. These three molecules are therefore examples of the three different possible types of band bending achievable in these ternary systems: constant band bending at minimum and maximum value and band bending pinning at a predesigned value with a small residual doping dependence for higher doping concentrations.

In summary, we have shown that self-assembled monolayers can limit band bending at interfaces between inorganic

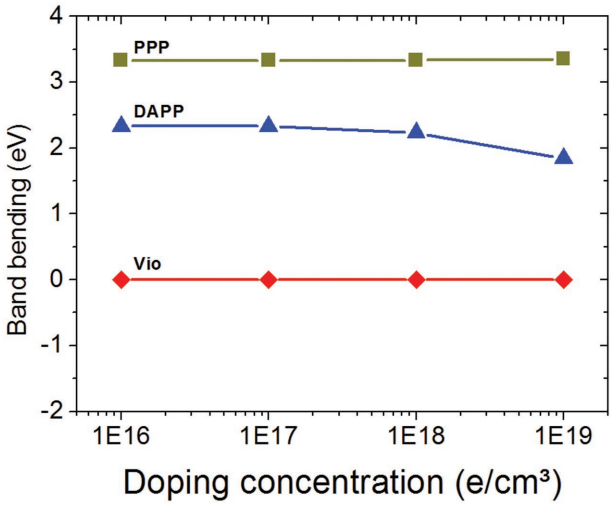

Figure 7. Band bending after TCNQ adsorption on ZnO/SAM, as function of the ZnO doping concentration.

electrodes and organic electronic acceptors. The maximum amount of band bending can be tuned by tuning the HOMO energy of the employed SAM. Particularly strong electron acceptors, such as Viologen, are even able to suppress band bending completely. SAMs with a HOMO in the gap pin the band bending at a predetermined energy, akin to deep donor states. Conversely, adsorbates with their HOMO below the valence-band maximum do not have any impact on the magnitude of the band bending.

Our results indicate that the toolbox of organic chemistry can be used to design surface-modifications, which generally mitigate or even completely suppress the occurrence of band bending in transparent conductive oxides. We expect that the application of such molecules makes the performance of organic electronic devices less dependent on unintentional doping during the crystal growth process or to changes of the doping concentration during device operations. Such devices may exhibit a better device performance and a better long-term stability.

3. Experimental Section

Calculations were performed using the FHI-aims code[46,47] with a numerically tabulated atomic orbital basis. Surfaces and interfaces were modeled by periodic slabs containing four double-layers of ZnO. A Gamma-centered k-grid of 16 × 16 × 1 points per ZnO unit cell was used and scaled appropriately to larger supercells. A region of at least 30 Å vacuum was inserted between the slab and its periodic replica. In the direction perpendicular to the surface, dipole interactions between repeated slabs were prevented by using a dipole correction.[48] FHI-aims' "tight" numerical settings were used, which also implied a "Tier 1" basis for Zn and a "Tier 2" basis for all other atoms. The electronic structure was calculated using the HSE06 functional[27,28] with 40% instead of the usual 25% exact exchange. The same amount of exact exchange was used in previous studies,[8,30] and similar values (37.5%) have been used by others.[29,49] All geometry optimizations were performed using the Perdew, Becke, and Ernzerhof[50] generalized gradient approximation corresponding to HSE with 0% exact exchange. To account for long-range van der Waals forces, we employed the vdW-TS scheme.[31] For ZnO, the parameters were obtained from time-dependent density functional theory.[32] We used C_6 = 46.0183, α = 13.7743, r_0 = 2.818 for Zn and C_6 = 4.45343, α = 4.28501, r_0 = 2.953 for O, as previously published in ref. [25]. The self-consistent field cycle was converged to a threshold of 10^{-6} eV for the total energy and 10^{-3} eV for the sum of eigenvalues. All geometries were optimized until the remaining forces were smaller than 10^{-3} eV Å^{-1}.

Due to its low-lying valence band, bulk ZnO is always found to be n-type doped.[51] In the present work, we use a modified version of the CREST method to account for doping.[33,34] CREST treats a part of the substrate (the surface) within DFT, while the long-range electrostatic behavior (i.e., in particular the band bending) is captured semi-classically using a charged plate at the bottom of the slab. Within the quantum-mechanically treated substrate, we employ the virtual crystal approximation to model the free charge carriers.[30,35,52] Here, the oxygen atoms are replaced by an electrically neutral pseudo-atom that contains a core with a charge of $8 + \delta$ and the same number of electrons. The excess electrons go to the bottom of the conduction band.

Any band bending beyond the slab is modeled quasi-classically by using a charged plate. In short, the charge of the plate is computed by requiring that adsorbing a molecule on the upper side of the slab must not change the position of the Fermi-level (i.e., the work function) on the bottom side of the slab. The position of the charged plate is then determined from the overall charge and the doping concentration. A more detailed explanation will be given in a future publication. In contrast to the original formulation, the simplified version of CREST used in this paper requires only the dielectric constant ε of ZnO and the work function of the unperturbed slab as input. We used ε = 4 for ZnO. The work function of the unperturbed slab was determined from calculations without the adsorbate for each doping concentration separately. The CREST-approach is performed self-consistently and was converged to a work function accuracy of 100 meV.

Supporting Information

Supporting Information is available from the Wiley Online Library or from the author.

Acknowledgements

Funding by the FWF-projects J3258-N20 and P27868-N36 and the collaborative research center (SFB) 951 of the German Science Foundation is gratefully acknowledged. This work was supported by the Academy of Finland through its Centres of Excellence Programme under Project Nos. 251748 and 284621. The authors thank Georg Heimel, Ofer Sinai, and Leeor Kronik for fruitful discussions about the CREST method. The computational results presented have been achieved in part using the Vienna Scientific Cluster (VSC). This research used resources of the Argonne Leadership Computing Facility, which is a DOE Office of Science User Facility supported under Contract DE-AC02-06CH11357.

Received: September 12, 2016
Revised: November 12, 2016
Published online:

[1] M. S. White, D. C. Olson, S. E. Shaheen, N. Kopidakis, D. S. Ginley, *Appl. Phys. Lett.* **2006**, *89*, 143517.
[2] K. Takanezawa, K. Hirota, Q.-S. Wei, K. Tajima, K. Hashimoto, *J. Phys. Chem. C* **2007**, *111*, 7218.
[3] C.-H. Hsieh, Y.-J. Cheng, P.-J. Li, C.-H. Chen, M. Dubosc, R.-M. Liang, C.-S. Hsu, *J. Am. Chem. Soc.* **2010**, *132*, 4887.
[4] S. K. Hau, H.-L. Yip, H. Ma, A. K.-Y. Jen, *Appl. Phys. Lett.* **2008**, *93*, 233304.

[5] A. S. Komolov, P. J. Møller, J. Mortensen, S. A. Komolov, E. F. Lazneva, *Surf. Sci.* **2005**, *586*, 129.
[6] M. Gruenewald, L. K. Schirra, P. Winget, M. Kozlik, P. F. Ndione, A. K. Sigdel, J. J. Berry, R. Forker, J.-L. Brédas, T. Fritz, O. L. A. Monti. *J. Phys. Chem. C* **2015**, *119*, 4865.
[7] R. Schlesinger, Y. Xu, O. T. Hofmann, S. Winkler, J. Frisch, J. Niederhausen, A. Vollmer, S. Blumstengel, F. Henneberger, P. Rinke, M. Scheffler, N. Koch. *Phys. Rev. B* **2013**, *87*, 155311.
[8] Y. Xu, O. T. Hofmann, R. Schlesinger, S. Winkler, J. Frisch, J. Niederhausen, A. Vollmer, S. Blumstengel, F. Henneberger, N. Koch, P. Rinke, M. Scheffler. *Phys. Rev. Lett.* **2013**, *111*, 226802.
[9] S. Braun, W. R. Salaneck, M. Fahlman, *Adv. Mater.* **2009**, *21*, 1450.
[10] O. T. Hofmann, V. Atalla, N. Moll, P. Rinke, M. Scheffler, *New J. Phys.* **2013**, *15*, 123028.
[11] O. Dulub, L. A. Boatner, U. Diebold, *Surf. Sci.* **2002**, *519*, 201.
[12] H. Li, L. K. Schirra, J. Shim, H. Cheun, B. Kippelen, O. L. A. Monti, J.-L. Bredas, *Chem. Mater.* **2012**, *24*, 3044.
[13] L. L. Kelly, D. A. Racke, P. Schulz, H. Li, P. Winget, H. Kim, P. Ndione, A. K. Sigdel, J.-L. Brédas, J. J. Berry, S. Graham, O. L. A. Monti, *J. Phys. Condens. Matter* **2016**, *28*, 94007.
[14] H. Ishii, K. Sugiyama, D. Yoshimura, E. Ito, Y. Ouchi, K. Seki, *IEEE J. Sel. Top. Quantum Electron.* **1998**, *4*, 24.
[15] R. J. Murdey, W. R. Salaneck, *Jpn. J. Appl. Phys.* **2005**, *44*, 3751.
[16] I. Avilov, V. Geskin, J. Cornil, *Adv. Funct. Mater.* **2009**, *19*, 624.
[17] S. Braun, X. Liu, W. R. Salaneck, M. Fahlman, *Org. Electron.* **2010**, *11*, 212.
[18] T. Mori, *Chem. Lett.* **2011**, *40*, 428.
[19] V. Atalla, M. Yoon, F. Caruso, P. Rinke, M. Scheffler, *Phys. Rev. B* **2013**, *88*, 165122.
[20] H. Skulason, C. D. Frisbie, *Langmuir* **1998**, *14*, 5834.
[21] C. Santato, F. Rosei, *Nat. Chem.* **2010**, *2*, 344.
[22] J. I. Martínez, E. Abad, F. Flores, J. Ortega, *Phys. Status Solidi B* **2011**, *248*, 2044.
[23] J. Walsh, R. Davis, C. Muryn, G. Thornton, V. Dhanak, K. Prince, *Phys. Rev. B* **1993**, *48*, 14749.
[24] S. Hövel, C. Kolczewski, M. Wühn, J. Albers, K. Weiss, V. Staemmler, C. Wöll, *J. Chem. Phys.* **2000**, *112*, 3909.
[25] O. T. Hofmann, J.-C. Deinert, Y. Xu, P. Rinke, J. Stähler, M. Wolf, M. Scheffler, *J. Chem. Phys.* **2013**, *139*, 174701.
[26] O. T. Hofmann, D. A. Egger, E. Zojer, *Nano Lett.* **2010**, *10*, 4369.
[27] J. Heyd, G. E. Scuseria, M. Ernzerhof, *J. Chem. Phys.* **2003**, *118*, 8207.
[28] A. V. Krukau, O. A. Vydrov, A. F. Izmaylov, G. E. Scuseria, *J. Chem. Phys.* **2006**, *125*, 224106.
[29] F. Oba, A. Togo, I. Tanaka, *Phys. Rev. B* **2008**, *77*, 245202.
[30] N. Moll, Y. Xu, O. T. Hofmann, P. Rinke, *New J. Phys.* **2013**, *15*, 83009.
[31] A. Tkatchenko, M. Scheffler, *Phys. Rev. Lett.* **2009**, *102*, 73005.
[32] G.-X. Zhang, A. Tkatchenko, J. Paier, H. Appel, M. Scheffler, *Phys. Rev. Lett.* **2011**, *107*, 245501.
[33] O. Sinai, O. T. Hofmann, P. Rinke, M. Scheffler, G. Heimel, L. Kronik, *Phys. Rev. B* **2015**, *91*, 75311.
[34] S. Erker, N. Moll, P. Rinke, O.T. Hofmann, unpublished.
[35] M. Scheffler, *Physica B+C* **1987**, *146*, 176.
[36] D. C. Look, D. C. Reynolds, J. R. Sizelove, R. L. Jones, C. W. Litton, G. Cantwell, W. C. Harsch, *Solid State Commun.* **1998**, *105*, 399.
[37] T. Lu, T. M. Cotton, R. L. Birke, J. R. Lombardi, *Langmuir* **1989**, *5*, 406.
[38] H.-H. Yang, R. L. McCreery, *Anal. Chem.* **1999**, *71*, 4081.
[39] Y. S. Park, S. Y. Um, K. B. Yoon, *J. Am. Chem. Soc.* **1999**, *121*, 3193.
[40] O. T. Hofmann, G. M. Rangger, E. Zojer, *J. Phys. Chem. C* **2008**, *112*, 20357.
[41] U. Özgür, Y. I. Alivov, C. Liu, A. Teke, M. A. Reshchikov, S. Doğan, V. Avrutin, S.-J. Cho, H. A. Morkoç, *J. Appl. Phys.* **2005**, *98*, 41301.
[42] S. Duhm, G. Heimel, I. Salzmann, H. Glowatzki, R. L. Johnson, A. Vollmer, J. P. Rabe, N. Koch, *Nat. Mater.* **2008**, *7*, 326.
[43] O. T. Hofmann, P. Rinke, M. Scheffler, G. Heimel, *ACS Nano* **2015**, *9*, 5391.
[44] J. P. Perdew, A. Ruzsinszky, L. A. Constantin, J. Sun, G. I. Csonka, *J. Chem. Theory Comput.* **2009**, *5*, 902.
[45] D. Hofmann, S. Kümmel, *Phys. Rev. B* **2012**, *86*, 201109.
[46] V. Blum, R. Gehrke, F. Hanke, P. Havu, V. Havu, X. Ren, K. Reuter, M. Scheffler, *Comput. Phys. Commun.* **2009**, *180*, 2175.
[47] S. V. Levchenko, X. Ren, J. Wieferink, R. Johanni, P. Rinke, V. Blum, M. Scheffler, *Comput. Phys. Commun.* **2015**, *192*, 60.
[48] J. Neugebauer, M. Scheffler, *Phys. Rev. B* **1992**, *46*, 16067.
[49] A. Janotti, J. B. Varley, P. Rinke, N. Umezawa, G. Kresse, C. G. Van de Walle, *Phys. Rev. B* **2010**, *81*, 85212.
[50] J. P. Perdew, K. Burke, M. Ernzerhof, *Phys. Rev. Lett.* **1996**, *77*, 3865.
[51] A. Janotti, C. G. Van de Walle, *Phys. Rev. B* **2007**, *76*, 165202.
[52] N. A. Richter, S. Sicolo, S. V. Levchenko, J. Sauer, M. Scheffler, *Phys. Rev. Lett.* **2013**, *111*, 45502.